Pushing the limits of sensitivity and resolution for natural abundance ^{43}Ca NMR using ultra-high magnetic field (35.2 T)†

Christian Bonhomme,*[a] Xiaoling Wang,[b] Ivan Hung,[b] Zhehong Gan,[b] Christel Gervais,[a] Capucine Sassoye,[a] Jessica Rimsza,[c] Jincheng Du,[c] Mark E. Smith,[d] John V. Hanna,[e] Stéphanie Sarda,[f] Pierre Gras,[g] Christèle Combes[g] and Danielle Laurencin*[h]

Natural abundance ^{43}Ca solid state NMR experiments are reported for the first time at ultra-high magnetic field (35.2 T) on a series of Ca-(pyro)phosphate and Ca-oxalate materials, which are of biological relevance in relation to biomineralization processes and the formation of pathological calcifications. The significant gain in both sensitivity and resolution at 35.2 T leads to unprecedented insight into the structure of both crystalline and amorphous phases.

Calcium is an element of major importance, due to its abundance in living organisms and tissues (*e.g.* bone and teeth), in natural rock-forming minerals (*e.g.* francolite, calcite, and dolomite), and in major construction materials (*e.g.* cement, concrete, glass and plaster). However, determining the local environment of this element within complex molecular and materials systems is far from trivial. In particular, structural analysis by ^{43}Ca NMR spectroscopy is highly challenging, due to the poor receptivity of the NMR-active isotope.[1] Calcium-43 is indeed a spin-7/2 quadrupolar nucleus of very low natural abundance (0.14%) and resonance frequency ($\nu_0(^{43}\mathrm{Ca})$ = 57.2 MHz at B_0 = 20 T).

To tackle sensitivity issues, two main approaches have been used in the field of ^{43}Ca solid state NMR.[1–3] The first consists in analyzing large quantities of sample (typically $\geq$300 mg) at high magnetic field (14 to 21 T NMR instruments) under moderate magic angle spinning (MAS) conditions.[1–4] However, even when using signal enhancement NMR sequences for quadrupolar nuclei,[1,5] several hours of acquisition are needed to record a 1D spectrum, which excludes *de facto* the implementation of 2D experiments. Moreover, large quantities of material are not always available, making this approach inapplicable for many systems. The second possibility is to label in ^{43}Ca the compounds of interest.[1,5,6] However, although the gain in sensitivity allows high resolution 1D and 2D correlation experiments to be performed, the major drawback is the high cost of the isotopically-enriched precursor ($\sim$1500 € for 10 mg of 60% ^{43}Ca-labeled $CaCO_3$). Moreover, it implies that synthetic protocols often have to be re-adapted to start from ^{43}Ca-enriched $CaCO_3$ as a calcium source.

The main challenge today for ^{43}Ca solid state NMR is to find means to reach a much higher sensitivity in order to be able to perform high resolution experiments at natural abundance on a broader variety of materials. In this context, the feasibility of DNP (Dynamic Nuclear Polarization)-enhanced $\{^1\mathrm{H}\}$–^{43}Ca CP (Cross Polarization) MAS experiments at natural abundance was recently demonstrated by Lee *et al.* on a 400 MHz instrument (B_0 = 9.4 T).[7] Such DNP analyses are nevertheless constrained by specific experimental features, like the need to find efficient impregnation conditions for each material and to perform measurements at low temperatures. Moreover, the quadrupolar nature of ^{43}Ca actually calls for performing measurements at higher fields to achieve better resolution, because the second-order quadrupolar broadening scales as $1/B_0$. Hence, the possibility of recording natural abundance ^{43}Ca MAS NMR spectra at much higher magnetic fields was investigated. In this article, the first natural abundance ^{43}Ca NMR study at 35.2 T (1.5 GHz ^{1}H Larmor frequency) are reported, using the series-connected hybrid (SCH) magnet at the US National High Magnetic Field Laboratory.[8]

As the SCH magnet is available for a restricted period of time per day ($\sim$7 hours), experiments were first set up by using a ^{43}Ca-labeled monetite sample (*$CaHPO_4$). The radiofrequency (RF) power on the ^{43}Ca channel was optimized for best efficiency of the multi-DFS (double frequency sweep) signal enhancement pulse sequence (final gain in signal-to-noise: $\sim$2).[5]

[a] *Sorbonne Université, CNRS, Collège de France, Laboratoire de Chimie de la Matière Condensée de Paris, LCMCP, F-75005 Paris, France. E-mail: christian.bonhomme@upmc.fr*
[b] *National High Magnetic Field Laboratory, 1800 East Paul Dirac Drive, Tallahassee, FL 32310-3706, USA*
[c] *Department of Materials Science and Engineering, University of North Texas, Denton, Texas 76207, USA*
[d] *Department of Chemistry, Lancaster University, Lancaster LA1 4YB, UK*
[e] *Department of Physics, Warwick University, Coventry, CV4 7AL, UK*
[f] *CIRIMAT, Université de Toulouse, CNRS, Université Paul Sabatier, 4 allée E. Monso, 31030 Toulouse cedex 4, France*
[g] *CIRIMAT, Université de Toulouse, CNRS, INPT – Ensiacet, 4 allée E. Monso, 31030 Toulouse cedex 4, France*
[h] *ICGM, UMR 5253, CNRS-UM-ENSCM, Place E. Bataillon, CC1701, 34095 Montpellier cedex 05, France. E-mail: danielle.laurencin@umontpellier.fr*

† Electronic supplementary information (ESI) available. See DOI: 10.1039/c8cc05193c

Moreover, measurements on *$CaHPO_4$ were repeated on different days using a modified/enhanced Bruker lock system, showing no detectable variation in frequency, which demonstrates the reliability of comparisons made on spectra recorded on different days. All NMR experimental parameters (including temperature, MAS probe, pulse schemes, relaxation delays, number of scans and procedure for chemical shift referencing[9]) are given in the ESI.†

Measurements on *$CaHPO_4$ illustrate the significant gain *in resolution* which is achieved at 35.2 T (Fig. 1a). Indeed, two resonances are clearly resolved at this field, and a second-order quadrupolar lineshape is even observed for the most deshielded signal, which was not the case at lower fields ($\leq$20.0 T) due to the strong overlap between resonances. The NMR parameters $\{\delta_{iso}, C_Q, \eta_Q\}$ of the two resonances were extracted by simulations at both fields. Given that the monetite structure actually exhibits 4 different Ca sites, a shifted-echo 3QMAS experiment was performed aiming at further ^{43}Ca resolution. The 2D spectrum could be recorded in just $\sim$50 minutes with a very good signal to noise ratio, due to the significant gain in sensitivity at 35.2 T (Fig. 1b). However, only two isotropic chemical shifts were observed in the f1 (indirect) dimension. According to GIPAW-DFT[10] (Gauge Including Projector Augmented Wave-Density Functional Theory) calculations on the monetite structure, this can be explained by the fact that the four inequivalent Ca sites can be divided in two groups exhibiting very similar ^{43}Ca NMR parameters, with the following averaged values:[9] $\{^{calc,avg}\delta_{iso}(^{43}Ca) = 4.2$ ppm, $^{calc,avg}C_Q(^{43}Ca) = -2.3$ MHz, $^{calc,avg}\eta_Q(^{43}Ca) = 0.40\}$ and $\{^{calc,avg}\delta_{iso}(^{43}Ca) = -4.4$ ppm $^{calc,avg}C_Q(^{43}Ca) = 1.4$ MHz, $^{calc,avg}\eta_Q(^{43}Ca) = 0.59\}$. Although this provides an explanation of the observed spectrum, understanding in detail the remaining discrepancy between these calculated average parameters and the experimental ones is still under study, and beyond the scope of the present article. Indeed, careful analyses of both the structural model of monetite and the computational approach used (including the choice of shielding reference, which is difficult to determine accurately) will need to be performed for this.

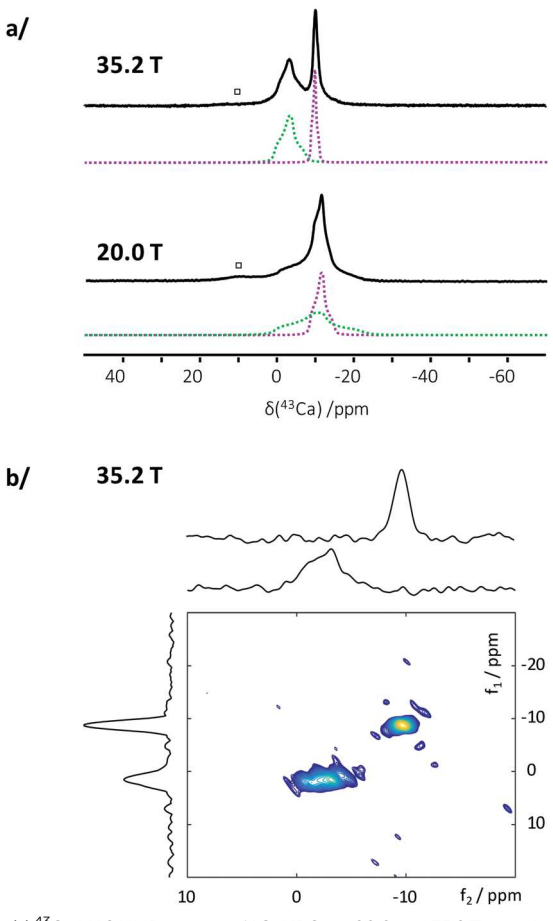

Fig. 1 (a) ^{43}Ca MAS NMR spectra of *$CaHPO_4$ at 20.0 and 35.2 T, together with their fit considering two average Ca environments $\{\delta_{iso}(^{43}Ca) = 0.7 \pm 0.8$ ppm; $|^{exp}C_Q(^{43}Ca)| = 3.5 \pm 0.3$ MHz, $^{exp}\eta_Q(^{43}Ca) = 0.8 \pm 0.1\}$, and $\{\delta_{iso}(^{43}Ca) = -8.5 \pm 0.8$ ppm; $|^{exp}C_Q(^{43}Ca)| = 1.8 \pm 0.3$ MHz, $^{exp}\eta_Q(^{43}Ca) = 0.8 \pm 0.1\}$ (□ corresponds to a minor impurity); (b) ^{43}Ca 3QMAS spectrum of *$CaHPO_4$ at 35.2 T.

With the gains in both sensitivity and resolution at 35.2 T, natural abundance ^{43}Ca MAS NMR experiments were carried out on $\sim$30 mg of crystalline calcium pyrophosphate and oxalate compounds (Fig. 2). In less than 4 hours, highly resolved spectra were obtained, while more than 5 hours and larger quantities of sample ($\sim$300 mg) had been needed previously at 20.0 T to study these phases.[2,3] Most importantly, for monoclinic calcium pyrophosphate tetrahydrate beta (m-$Ca_2P_2O_7{\cdot}4H_2O$, noted also m-CPPT β) and calcium oxalate monohydrate ($CaC_2O_4{\cdot}H_2O$, noted also COM), for which the two crystallographic Ca sites were barely resolved at 20.0 T (the isotropic chemical shifts being separated by less than 3.5 ppm),[2,3] clear resolution was achieved at 35.2 T. In contrast, for the triclinic calcium pyrophosphate dihydrate phase (t-$Ca_2P_2O_7{\cdot}2H_2O$, noted also t-CPPD), in which the ^{43}Ca isotropic shifts are separated by less than 2.5 ppm and the quadrupolar coupling constants are slightly larger ($|C_Q| \sim 3$ MHz), the two sites are not resolved. More generally, for ^{43}Ca sites characterized by $C_Q(^{43}Ca) \leq 3$ MHz, second-order quadrupolar broadening effects are almost absent at 35.2 T, and the breadth of the signals is hence a reflection of the distribution in isotropic chemical shifts and/or the intrinsic relaxation of ^{43}Ca. This is obviously the case for the COM sample (Fig. 2).

Based on the encouraging measurements made on the crystalline Ca-pyrophosphate and oxalate phases (Fig. 2), the characterization of an amorphous pyrophosphate phase $Ca_2P_2O_7{\cdot}xH_2O$ (a-CPP, $x \sim 4$) at 35.2 T was undertaken. This sample represented a much greater challenge for natural abundance ^{43}Ca NMR, due to wider range of variation of the chemical shift and quadrupolar NMR parameters, which lead to broader signals.[2] Moreover, given that Ca-sites with large quadrupolar coupling constants ($|C_Q(^{43}Ca)| > 5.5$ MHz) may be found in amorphous materials,[11] natural abundance ^{43}Ca MAS NMR measurements at "lower" fields ($B_0 \leq 20$ T) using spinning speeds of $\sim$5 kHz (which is in practice the upper limit for some of the commercial large volume rotors) could actually lead to misleading lineshapes. As a matter of fact, very few data related to calcium-containing glasses (labeled in ^{43}Ca),[12,13] and amorphous derivatives (in natural abundance) have been published so far.[1,2]

The natural abundance ^{43}Ca MAS NMR spectrum of a-CPP was recorded at 35.2 T (Fig. 3a). Thanks to the very fast relaxation

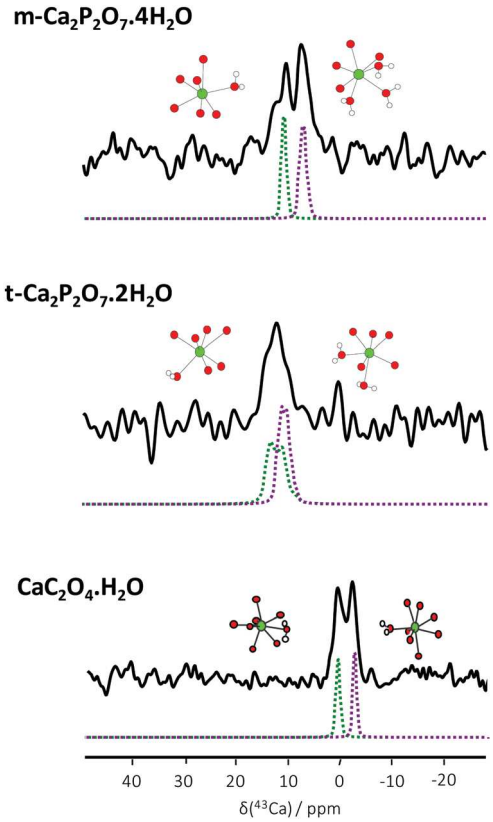

Fig. 2 Natural abundance ^{43}Ca MAS NMR spectra of m-$Ca_2P_2O_7{\cdot}4H_2O$ (m-CPPT β, 2.5 hours), t-$Ca_2P_2O_7{\cdot}2H_2O$ (t-CPPD, 3 hours) and $CaC_2O_4{\cdot}H_2O$ (COM, 3 hours), recorded at 35.2 T. The dashed lines show the simulation of the contributions of the two inequivalent Ca-sites in each structure, using the experimental ^{43}Ca NMR parameters determined previously (which are recalled in ESI† in Table S2).[2,3]

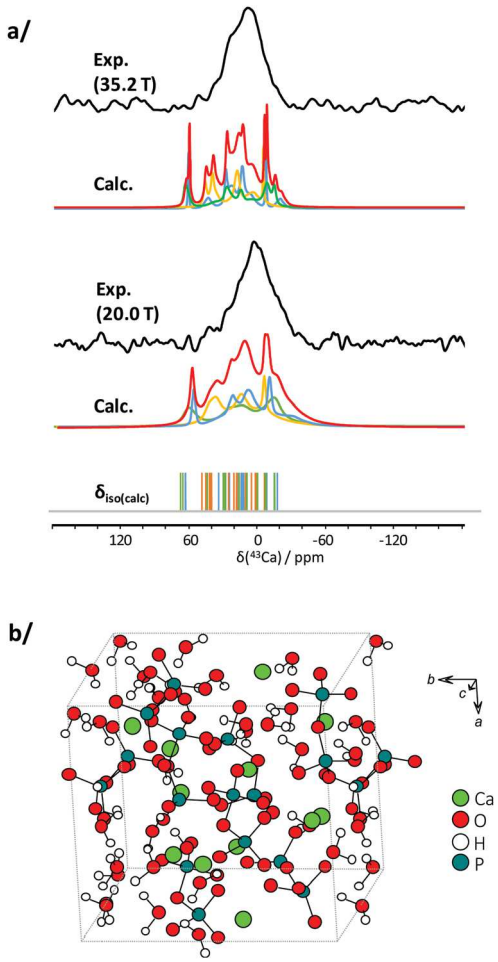

Fig. 3 (a) ^{43}Ca MAS NMR spectra of amorphous-$Ca_2P_2O_7{\cdot}4H_2O$ (a-CPP) at 20.0 and 35.2 T, together with the GIPAW-DFT ^{43}Ca NMR calculations related to the three AIMD derived models (sum in red, contributions of models I, II and III in blue, orange and green respectively; calculated isotropic shifts are shown as vertical bars); (b) AIMD derived computational model of a-CPP (model I) used for DFT calculations (see ESI† for further details as each of three models provides 12 calcium sites).

of ^{43}Ca in the sample, less than 4 hours were needed to record the spectrum, which is all the more remarkable when considering that the signal is ~10 times broader in comparison to those of the crystalline phases reported above.

In order to gain greater 'chemical insight' into the origin of these distributions, computational models of the amorphous compound were developed, using Monte Carlo (MC) based simulations with bond constraints followed by relaxation with *Ab Initio* Molecular Dynamics (AIMD) simulations and geometry optimization with DFT calculations (see ESI†). It should be noted that in contrast to non-hydrated calcium derived glasses,[13] the commonly used melt-quench approach for MD could not be used to model amorphous $Ca_2P_2O_7{\cdot}4H_2O$, as it would have led to condensed phosphate chains with various lengths and would not have been able to tackle the presence of water molecules. Here, using combined MC, AIMD, and DFT calculations, three models of this amorphous phase with hydrated calcium pyrophosphate groups were generated (each with 12 Ca sites, see Fig. 3b).‡ For each model, calculated Pair Distribution Function (PDF) analyses were compared to the experimental data, showing that the agreement is reasonable (Fig. S3 in ESI†).

The analysis of the Ca local environments in these models demonstrates that (i) coordination numbers range between 4 and 9, (ii) up to 5 water molecules can be bound to Ca^{2+}, and (iii) the average Ca···O bond distances are between 2.3 and 2.6 Å (see ESI,† Table S4). These values are in agreement with the structural parameters of the crystalline calcium pyrophosphate phases (dihydrate and tetrahydrate). Coordination numbers range from 6 to 7 for calcium atoms in these structures and bond distances are between 2.257 and 2.668 Å.[14–16] DFT calculations of the ^{43}Ca NMR parameters were then carried out, using the GIPAW-DFT approach (see ESI† for computational details). The range of variation of the calculated isotropic chemical shift (-16.1 ppm $< {}^{calc}\delta_{iso}(^{43}Ca) <$ 64.3 ppm; average value of 21.6 ppm) and quadrupolar coupling constants (1.2 MHz $< |{}^{calc}C_Q(^{43}Ca)| <$ 6.5 MHz; average value of 3.4 MHz) is consistent with the experimental data (Fig. 3a). More specifically, it is worth noting that the calculated values ${}^{calc}\delta_{iso}(^{43}Ca)$ spread out across the experimental lineshape obtained at 35.2 T, with more of the calculated values positioned towards where the signal has maximum intensity. Despite the lack of sufficient statistics at

this stage, which are visible from the simulated sums of the models (Fig. 3a, red curves), these AIMD models appear as the first realistic starting point for describing Ca local environments in these amorphous materials. In Fig. S4 (ESI†), additional simulations including Czjzek distributions of quadrupolar parameters (Gaussian Isotropic Model, GIM) as well as Gaussian distributions of ^{43}Ca isotropic chemical shifts[17] are presented, which show that at ultra-high magnetic field, it is likely that simple distributions of isotropic chemical shifts are mainly observed. Finally, it should be noted that GIPAW NMR calculations were performed at 0 K, therefore not taking into account potential local dynamics of the water molecules,[2] which could affect the ^{43}Ca NMR parameters. Low temperature ^{43}Ca NMR experiments will need to be performed in the future to investigate this aspect.

All in all, the 1.5 GHz series connected hybrid instrument paves new avenues for natural abundance ^{43}Ca MAS NMR. Significant gains in both resolution and sensitivity were demonstrated in the case of crystalline calcium pyrophosphate and oxalate phases. Most importantly, thanks to favorable relaxation characteristics, the natural abundance ^{43}Ca MAS NMR spectrum of an amorphous hydrated calcium pyrophosphate was successfully obtained, which could be compared for the first time to models generated by AIMD computer simulations of this phase. This point is of crucial importance as amorphous precursors of calcium carbonate,[18] calcium oxalate[19] and calcium (pyro)phosphates[20] are meant to play a fundamental role in biomineralization processes, which have not been fully characterized so far (notably regarding Ca environments). Moreover, such ^{43}Ca NMR experiments at ultra-high magnetic field may also provide complementary clues regarding the polyamorphism of biomaterials.[2,21]

The French National Research Agency (ANR) is acknowledged for financial support (“CAPYROSIS” project – ANR-12-BS08-0022-01; “PYVERRES” project – ANR-16-CE19-0013). A portion of this work was performed at the National High Magnetic Field Laboratory, which is supported by the National Science Foundation Cooperative Agreement No. DMR-1157490 & DMR-1644779, and the State of Florida. JD acknowledges financial support of National Science Foundation (NSF) Ceramics Program DMR-1508001. The UK 850 MHz solid-state NMR Facility used in this research was funded by EPSRC and BBSRC (contract PR140003), as well as the University of Warwick including part funding through Birmingham Science City Advanced Materials Projects 1 and 2 supported by Advantage West Midlands (AWM) and the European Regional Development Fund (ERDF). NMR spectroscopic calculations were performed using HPC resources from GENCI-IDRIS (Grant 097535).

Conflicts of interest

There are no conflicts to declare.

Notes and references

‡ Due to the high computational cost of the AIMD simulations (see ESI† for further details), only 3 models of the a-CPP phase have been generated so far, with a general formula $Ca_2P_2O_7{\cdot}4H_2O$. It should be noted that in the amorphous phases characterized experimentally, the pyrophosphate content is slightly lower ($\sim$3.5–3.9 H_2O per pyrophosphate).

1 C. M. Widdifield, *Annu. Rep. NMR Spectrosc.*, 2017, **92**, 227; D. Laurencin and M. E. Smith, *Prog. Nucl. Magn. Reson. Spectrosc.*, 2013, **68**, 1; D. Bryce, *Dalton Trans.*, 2010, **39**, 8593.
2 P. Gras, A. Baker, C. Combes, C. Rey, S. Sarda, A. J. Wright, M. E. Smith, J. V. Hanna, C. Gervais, D. Laurencin and C. Bonhomme, *Acta Biomater.*, 2016, **31**, 348.
3 H. Colas, L. Bonhomme-Coury, C. Coelho Diogo, F. Tielens, F. Babonneau, C. Gervais, D. Bazin, D. Laurencin, M. E. Smith, J. V. Hanna, M. Daudon and C. Bonhomme, *CrystEngComm*, 2013, **15**, 8840.
4 S. Chen, B. E. G. Lucier, M. Chen, V. V. Terskikh and Y. Huang, *Chem. – Eur. J.*, 2018, **24**, 8732.
5 K. M. N. Burgess, F. A. Perras, I. L. Moudrakovski, Y. Xu and D. L. Bryce, *Can. J. Chem.*, 2015, **93**, 799.
6 D. Laurencin, A. Wong, J. V. Hanna, R. Dupree and M. E. Smith, *J. Am. Chem. Soc.*, 2008, **130**, 2412; A. Wong, D. Laurencin, R. Dupree and M. E. Smith, *Solid State Nucl. Magn. Reson.*, 2009, **35**, 32; D. Laurencin, C. Gervais, A. Wong, C. Coelho, F. Mauri, D. Massiot, M. E. Smith and C. Bonhomme, *J. Am. Chem. Soc.*, 2009, **131**, 13430.
7 D. Lee, C. Leroy, C. Crevant, L. Bonhomme-Coury, F. Babonneau, D. Laurencin, C. Bonhomme and G. De Paëpe, *Nat. Commun.*, 2017, **8**, 14104.
8 Z. Gan, I. Hung, X. L. Wang, J. Paulino, G. Wu, I. M. Litvak, P. L. Gor'kov, W. W. Brey, P. Lendi, J. L. Schiano, M. D. Bird, L. R. Dixon, J. Toth, G. S. Boebinger and T. A. Cross, *J. Magn. Reson.*, 2017, **284**, 125.
9 C. Gervais, D. Laurencin, A. Wong, F. Pourpoint, J. Labram, B. Woodward, A. P. Howes, K. J. Pike, R. Dupree, F. Mauri, C. Bonhomme and M. E. Smith, *Chem. Phys. Lett.*, 2008, **464**, 42.
10 C. J. Pickard and F. Mauri, *Phys. Rev. B: Condens. Matter Mater. Phys.*, 2001, **63**, 245101.
11 A. Pedone, T. Charpentier and M. C. Menziania, *Phys. Chem. Chem. Phys.*, 2010, **12**, 6054.
12 K. Shimoda, Y. Tobu, Y. Shimoikeda, T. Nemoto and K. Saito, *J. Magn. Reson.*, 2007, **186**, 156; F. Angeli, M. Gaillard, P. Jollivet and T. Charpentier, *Chem. Phys. Lett.*, 2007, **440**, 324.
13 E. Gambuzzi, A. Pedone, M. C. Menziani, F. Angeli, P. Florian and T. Charpentier, *Solid State Nucl. Magn. Reson.*, 2015, **68–69**, 31.
14 N. S. Mandel, *Acta Crystallogr., Sect. B: Struct. Crystallogr. Cryst. Chem.*, 1975, **31**, 1730.
15 T. Balić-Žunić, M. R. Christoffersen and J. Christoffersen, *Acta Crystallogr., Sect. B: Struct. Sci.*, 2000, **56**, 953.
16 P. Gras, C. Rey, G. André, C. Charvillat, S. Sarda and C. Combes, *Acta Crystallogr., Sect. B: Struct. Sci., Cryst. Eng. Mater.*, 2016, **72**, 96.
17 D. R. Neuville, L. Cormier and D. Massiot, *Geochim. Cosmochim. Acta*, 2004, **68**, 5071.
18 Y. Wang, S. Von Euw, F. M. Fernandes, S. Cassaignon, M. Selmane, G. Laurent, G. Pehau-Arnaudet, C. Coelho, L. Bonhomme-Coury, M.-M. Giraud-Guille, F. Babonneau, T. Azaïs and N. Nassif, *Nat. Mater.*, 2013, **12**, 1144; S. Weiner, Y. Levi-Kalisman, S. Raz and L. Addadi, *Connect. Tissue Res.*, 2003, **44**, 24.
19 E. Ruiz-Agudo, A. Burgos-Cara, C. Ruiz-Agudo, A. Ibanez-Velasco, H. Cölfen and C. Rodriguez-Navarro, *Nat. Commun.*, 2017, **8**, 768.
20 K. Ley-Ngardigal, C. Combes, S. Teychene, C. Bonhomme, C. Coelho-Diogo, P. Gras, C. Rey and B. Biscans, *Cryst. Growth Des.*, 2017, **17**, 37.
21 J. H. E. Cartwright, A. G. Checa, J. D. Gale, D. Gebauer and C. I. Sainz-Diaz, *Angew. Chem.*, 2012, **51**, 11960.

Pushing the limits of sensitivity and resolution for natural abundance ^{43}Ca NMR using ultra-high magnetic field (35.2 T)

Christian Bonhomme,*[a] Xiaoling Wang,[b] Ivan Hung,[b] Zhehong Gan,[b] Christel Gervais,[a] Capucine Sassoye,[a] Jessica Rimsza,[c] Jincheng Du,[c] Mark E. Smith,[d] John V. Hanna,[e] Stéphanie Sarda,[f] Pierre Gras,[g] Christèle Combes,[g] and Danielle Laurencin*[h]

[a.] *Sorbonne Université, CNRS, Collège de France, Laboratoire de Chimie de la Matière Condensée de Paris, LCMCP, F-75005 Paris, France (CB: christian.bonhomme@upmc.fr)*
[b.] *National High Magnetic Field Laboratory, 1800 East Paul Dirac Drive, Tallahassee, FL 32310–3706, USA.*
[c.] *Department of Materials Science and Engineering, University of North Texas, Denton, Texas 76207, USA*
[d.] *Department of Chemistry, Lancaster University, Lancaster LA1 4YB, UK*
[e.] *Department of Physics, Warwick University, Coventry, CV4 7AL, UK*
[f.] *CIRIMAT, Université de Toulouse, CNRS, Université Paul Sabatier,4 allée E. Monso, 31030 Toulouse cedex 4, France*
[g.] *CIRIMAT, Université de Toulouse, CNRS, INPT - Ensiacet, 4 allée E. Monso, 31030 Toulouse cedex 4, France*
[h.] *ICGM, UMR 5253, CNRS-UM-ENSCM, Place E. Bataillon, CC1701, 34095 Montpellier cedex 05, France (DL : danielle.laurencin@umontpellier.fr)*

Supporting Information

Synthetic procedures

The crystalline Ca-pyrophosphate phases, namely monoclinic calcium pyrophosphate tetrahydrate in the β phase (m-CPPT β, *m*-$Ca_2P_2O_7.4H_2O$), and triclinic calcium pyrophosphate dihydrate (t-CPPD, *t*-$Ca_2P_2O_7.2H_2O$), as well as the related amorphous compound referred to as a-CPP (composition $Ca_2P_2O_7.xH_2O$, with x ~ 4), were prepared as described in the literature.[1]

The crystalline Ca-oxalate monohydrate phase ($CaC_2O_4.H_2O$, COM) was synthesized according to a previously published procedure.[2]

The ^{43}Ca-labeled Ca-monetite phase was synthesized using $CaCO_3$ (partially enriched in ^{43}Ca) and H_3PO_4 as precursors. First, a mixture of 41 mg of ^{43}Ca-labeled $CaCO_3$ (60%-labelling, CortecNet) and 85 mg of non-labeled $CaCO_3$ (Aldrich) was heated to 1000°C under a flow of Ar.
After cooling to room temperature, ~70 mg of ^{43}Ca-enriched CaO were recovered (^{43}Ca-enrichment level ~20%). The labeled *CaO powder (~ 70 mg; n(Ca) ~ 1.25 mmol) was then transferred into a centrifuge tube, in which 1.5 mL of HPLC-grade water were added. The suspension was heated to 90°C under stirring (in an Ar atmosphere), before adding drop by drop 1.37 mL of a 1.00 mol.L^{-1} aqueous solution of H_3PO_4 (n(P) ~ 1.37 mmol). An additional 0.5 mL of HPLC-grade water was added to the medium, which was heated to 90°C for 3 days. Given that the goal of this synthesis was initially to prepare hydroxyapatite ($Ca_{10}(PO_4)_6(OH)_2$, Ca/P = 1.67), but that the "P" content initially added was too high, an additional amount of non-labelled Ca was then added after 3 days (in the form of an aqueous suspension of Ca-(hydr)oxide), in order to increase the Ca/P ratio in the reaction medium. Moreover, an additional amount of base (added under the form of an aqueous solution of NH_4OH) was then added. After 3 more days of stirring, the suspension was centrifuged, thoroughly washed several times with HPLC water, and then dried for 10 h at 100°C under vacuum. A total amount of 220 mg of precipitate was isolated.
The compound was then characterized by powder X-ray diffraction (Figure S1), showing that it mainly contains 2 crystalline phases ($CaHPO_4$ and $Ca(OH)_2$), and a small amount of hydroxyapatite. ^{43}Ca NMR analyses were then carried out, revealing that the ^{43}Ca NMR spectrum is similar to the previously reported data of $CaHPO_4$ (Figure S2).[3] The resonance of $Ca(OH)_2$ (δ_{iso} ~ 71 ppm; C_Q ~ 2.6 MHz) is not observed, meaning that this impurity is not significantly labeled (and hence not visible in ^{43}Ca NMR).

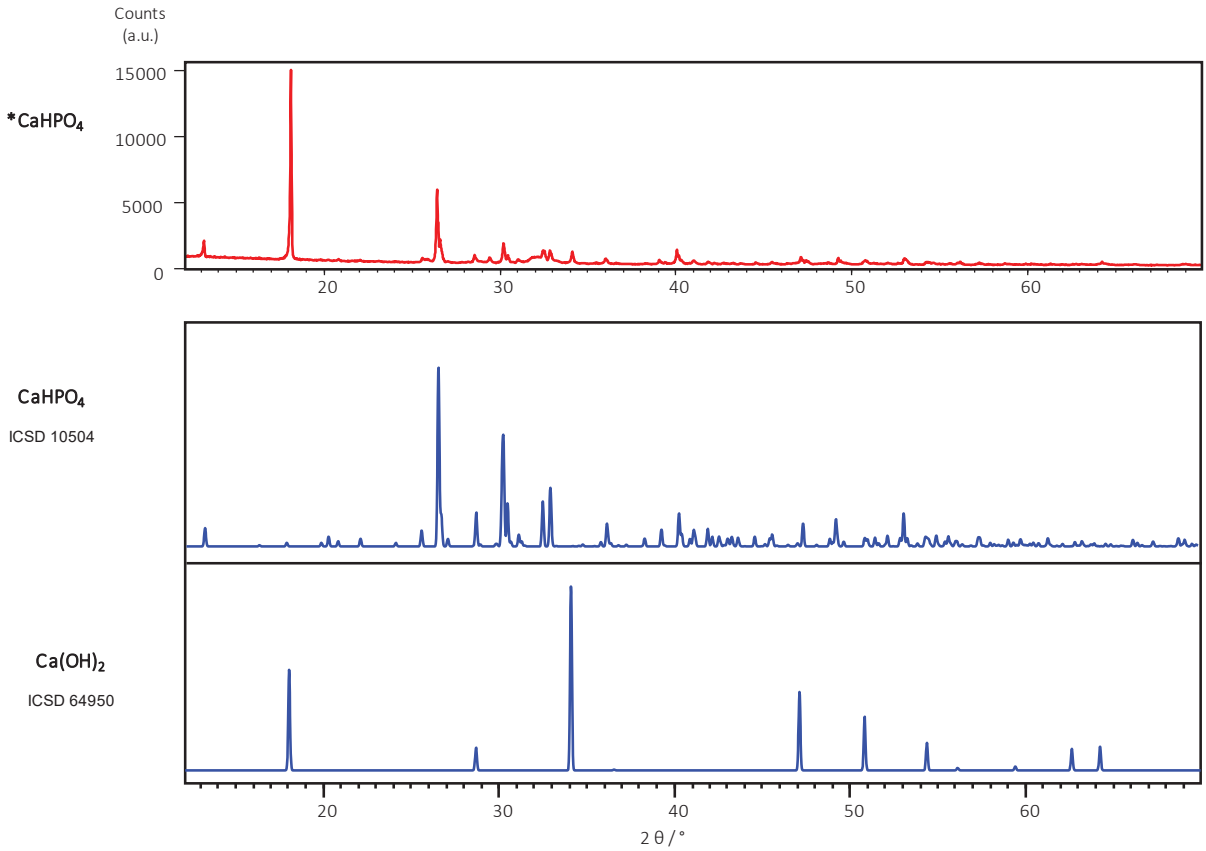

Figure S1. Experimental XRD powder pattern of the ^{43}Ca-enriched phase (top in red, *$CaHPO_4$), in comparison to published patterns for $CaHPO_4$ and $Ca(OH)_2$.

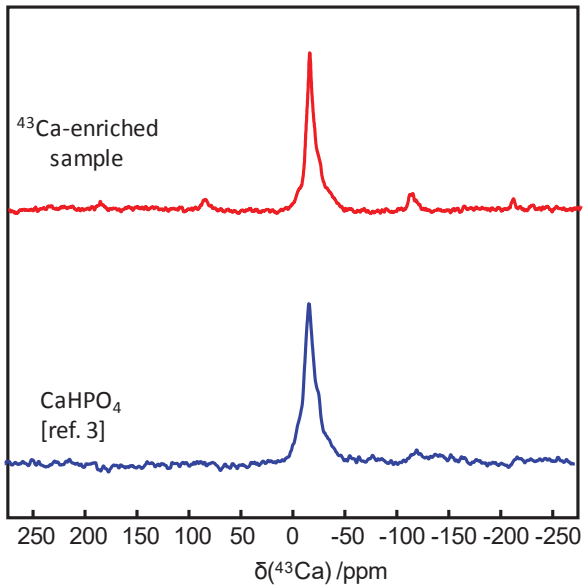

Figure S2. ^{43}Ca MAS NMR spectrum recorded at 14.1 T for the labeled phase (top), in comparison with the previously reported NMR spectrum of $CaHPO_4$ recorded at the same field at natural abundance (bottom).[3]

NMR acquisition parameters at 35.2 T

All experiments were carried out at 35.2 T, using a single-channel 3.2 mm MAS probe, tuned to ^{43}Ca ($\nu_0(^{43}Ca)$ = 100.96 MHz). Experiments were performed under temperature regulation (T = 283 K). Out of the five samples analyzed, only *$CaHPO_4$ was labeled in ^{43}Ca. Spectra were referenced to a 1.00 mol.L^{-1} solution of $CaCl_2$.

Table S1. Summary of the NMR acquisition parameters.

Sample	NMR sequence	Relaxation delay (s)	NS	total exp. time	ν_r (kHz)
*$CaHPO_4$	multi-dfs [(a)]	0.5	1k	3 min	10
*$CaHPO_4$	3Q echo shifted MQMAS [(b)]	0.5	96 *per* incr.	52 min	10
t-CPPD	multi-dfs[(a)]	0.5	114k	3 hours	18
m-CPPT β	wurst zg[(c)]	0.8	11k	2.5 hours	10
COM	zg	0.8	13k	3 hours	10
a-CPP	multi-dfs[(a)]	0.2	268k	3 hours	10

[(a)]4 blocks of DFS (optimized)[4], DFS pulse length: 5 ms (optimized), followed by a 90° selective pulse: 10 µs (at power level: 10 W – which corresponds to 6.25 kHz based on measurements on a solution of $CaCl_2$).
[(b)]excitation pulse: 3 µs – reconversion pulse: 1µs at power level: 400 W (39.5 kHz), echo delay: 982 µs (optimized), SPAM:[5] 90°: 6 µs at power level: 20W (8.8 kHz), 64 t_1 increments.
[(c)] WURST pulse[6]: 5 ms at power level: 13W (7.1 kHz).

It is worth mentioning that our attempts to record the *natural abundance* ^{43}Ca MAS NMR spectrum of a *highly crystalline* hydroxyapatite ($Ca_{10}(PO_4)_6(OH)_2$) were unsuccessful at this stage (despite the high $\%_{wt}$(Ca)). The hydroxyapatite sample analysed here was purchased from Biorad, and showed a very high crystallinity in X-Ray diffraction. This specific sample had not been studied by ^{43}Ca NMR at other fields before.
The main cause of this failure is most probably the long relaxation delay (due to the high crystallinity of the sample), as has been also noticed in the past for other Ca-compounds. Hence, the effect of relaxation has to be taken into account by users, as « overnight experiments » are not feasible currently at the ultra-high magnetic field facility.

Previously reported ^{43}Ca NMR parameters for the m-CPPT β, t-CPPD and COM crystalline phases

Table S2. Experimental *vs* calculated ^{43}Ca NMR parameters. For t-CPPD and m-CPPT β, unit cell parameters were fixed but proton positions were relaxed,[7] while for COM, both unit cell parameters and all atomic positions were relaxed.[2]

	Site	δ_{iso} (ppm)		C_Q (MHz)		η_Q	
		Exp	Calc	Exp	Calc	Exp	Calc
t-CPPD[7]	Ca1	14.5	13.8	3.4	−3.11	0.3	0.42
	Ca2	12.0	12.0	2.7	−2.47	0.5	0.14
m-CPPT β[7]	Ca1	11.0	11.9	1.8	1.57	0.6	0.43
	Ca2	7.5	11.4	2.1	2.36	0.6	0.67
COM[2]	Ca1	-2.6	-1.7	1.5	-1.34	0.6	0.99
	Ca2	0.7	4.2	1.6	1.68	0.7	0.59

Computational modeling: generation of models of the amorphous phase (a-CPP) by Ab Initio Molecular Dynamics (AIMD)

The development of amorphous calcium pyrophosphate (a-CPP) models is based on a multi-step protocol to ensure the development of isolated pyrophosphate anions (rather than phosphate chains or isolated orthophosphate ions), to which cations and water molecules are then added to generate an inverted glass structure. Initial placement of phosphorous atoms utilized a stochastic Monte Carlo (MC) process, as implemented in the RMCA code.[8]

Using an initial random mixture of 12 P atoms, MC was used to ensure a separation distance of 2.9-3.3 Å between the phosphate atoms. This is consistent with a P-P interatomic distance of ~ 2.9-3.0 Å, as reported in experimental pyrophosphate systems. Once this criterion had been satisfied, bridging oxygen atoms were placed between pairs of phosphorous atoms and radial oxygen were placed around the phosphate atoms to form a coordination number of four and generate the pyrophosphate species. The relaxation of the system was performed using periodic DFT calculations, starting with relaxation of the pyrophosphate systems alone (i.e. without including cations or water molecules). In this case, the charge of the systems due to the $P_2O_7^{4-}$ molecules was offset by the application of a background charge. The systems were relaxed to an energy minimum (~ 250 steps) and then systems were hydrated with water, and calcium cations were added at the appropriate ratio (Ca/P = 1). To confirm the density of the systems a cell optimization was performed to ensure the generation of systems at thermo-mechanical equilibrium at zero atmospheric pressure. This consisted of cell size optimization through which the cell dimensions were adjusted to identify the ideal density. A geometry optimization was performed between each cell optimization step to maintain the correct a-CPP structure. After the cell size optimization, *ab initio* molecular dynamics (AIMD) simulations for 5 ps (1 fs time step) were performed under the NVT ensemble at 300 K using a Nose-Hoover thermostat to further relax the generated structure models. A final geometry optimization step was performed following *AIMD* with an energy convergence of 1.0E-4 and a force convergence of 1.0E-3. Following the structural relaxation, a higher self-consistency accuracy (1E-10) relaxation before the GIPAW calculation was performed (discussed below).

Pair Distribution Function (PDF) analyses of a-CPP: comparison of experimental data to 3 computational models

In order to extract the Pair Distribution Function (PDF), X-Ray Diffraction (XRD) measurements were performed with a Bruker D8 ADVANCE diffractometer equipped with a LYNXEYE detector, with Mo Kα radiation (mean $\lambda(K_{\alpha 1 \alpha 2})$ = 0.71073Å) and a Zirconium filter, using the reflection mode. The final XRD pattern (Q_{min} = 1.08 $Å^{-1}$ and Q_{max} = 17 $Å^{-1}$) was obtained from the combination of 3 patterns measured with fixed divergence slit (0.3°) converted in counts per second with the following parameters $2\theta_i$(°)-$2\theta_f$(°)-step size(°)-step time(s): 7-50-0.05-25, 50-90-0.05-50 and 90-148-0.05-100.

The PDFgetX3 program[9] was used for the extraction of the PDF from the experimental XRD pattern (Figure S3), with the rpoly (limitation of the maximum frequency in the F(Q) correction polynomial) and Q_{max} (Q cutoff for the meaningful input intensities) parameters set to 1.63 and 16.6 respectively. PDF curves were also calculated from the 3 computational models using PDFGUI software[10]. Thermal displacements were fixed (U_{ii}=0.005$Å^2$). The particle size was here set at 15 Å in order to mimic the missing long range order of amorphous materials[11].

The experimental and calculated curves were then compared allowing the scale factor to vary for the best fit.

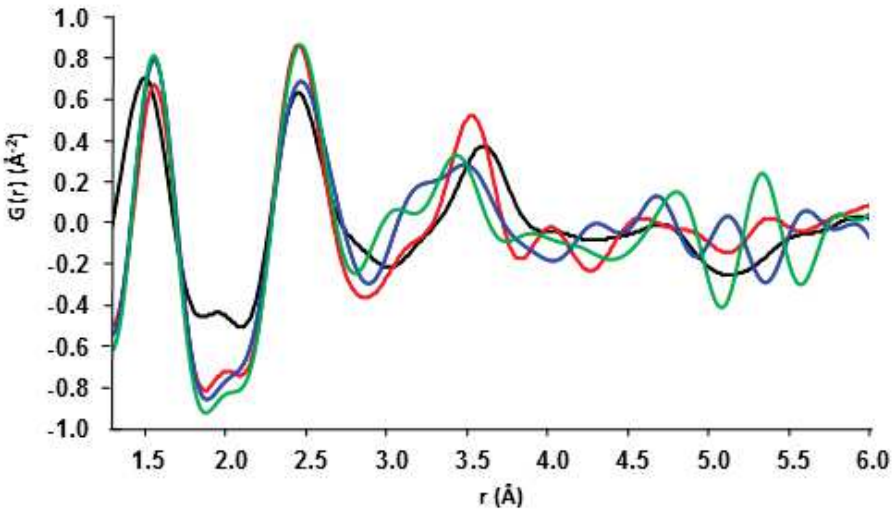

Figure S3. Experimental (black) and calculated (red for model I, blue for model II, green for model III) of the amorphous-$Ca_2P_2O_7.xH_2O$ phase (a-CPP, x ~ 4).

DFT calculation of the NMR parameters using the GIPAW approach

Computational NMR spectra were performed utilizing DFT electronic structure calculations based on the GIPAW method[12] and implemented in the Quantum Espresso code.[13] Norm-conserving pseudopotentials[14] in the Kleinman-Bylander form[15] with generalized gradient approximation (GGA) in the form of Perdew, Burke, and Ernzerhof (PBE)[16] was implemented. An energy cut-off of 80 Ry was used with a 1x1x1 k-point matrix based on the amorphous nature of the system. The initial structural models developed using the AIMD/DFT protocol described above were used as initial inputs and were re-optimized under described electronic structure conditions. Absolute shielding tensors for the computational systems were calculated from fully converged all-electron calculations. To set the ^{43}Ca chemical shift scale, as previously described, the calculated δ_{iso} for a series of reference compounds were compared to experimental values so that the average sum of experimental and calculated shifts coincide.[17] The principal components V_{xx}, V_{yy}, and V_{zz} of the electric field gradient (EFG) tensor were obtained by diagonalization of the traceless EFG tensor. The quadrupolar interaction can then be characterized by the quadrupolar coupling constant C_Q and the asymmetry parameter η_Q, which are defined as: $C_Q = eQV_{zz}/h$ and $\eta_Q = (V_{yy}-V_{xx})/V_{zz}$. The experimental value of the quadrupole moment of ^{43}Ca ($Q = -4.44 \times 10^{-30}$ m^2) was used to calculate C_Q.[18]

Table S3: GIPAW computed ^{43}Ca NMR parameters for the three models (including averages of $C_Q(^{43}Ca)$ and $\delta_{iso}(^{43}Ca)$.

	Model I			Model II			Model III		
	δ_{iso} (ppm)	C_Q (MHz)	η_Q	δ_{iso} (ppm)	C_Q (MHz)	η_Q	δ_{iso} (ppm)	C_Q (MHz)	η_Q
Ca1	-16.1	-3.84	0.85	-5.5	1.18	0.42	26.9	3.58	0.49
Ca2	46.7	-3.73	0.83	17.7	-2.27	0.51	42.0	4.64	0.60
Ca3	16.9	-3.50	0.46	38.8	-3.37	0.27	64.3	2.16	0.90
Ca4	28.5	2.15	0.92	24.5	4.86	0.30	28.3	-5.70	0.61
Ca5	14.1	-2.52	0.40	5.4	3.45	0.69	-14.1	-2.16	0.71
Ca6	13.5	-5.13	0.30	40.1	-2.05	0.76	-6.9	-2.78	0.63
Ca7	-7.4	-1.55	0.54	27.9	-5.53	0.58	62.3	2.84	0.26
Ca8	24.2	-3.49	0.59	46.7	-2.13	0.88	0.4	4.73	0.99
Ca9	60.6	-1.52	0.85	10.5	-3.82	0.40	15.7	-2.73	0.43
Ca10	12.2	4.60	0.82	19.8	2.36	0.75	9.3	4.24	0.52
Ca11	33.1	-6.54	0.88	43.6	3.76	0.47	28.6	2.66	0.83
Ca12	28.0	-3.67	0.70	1.9	-4.56	0.94	-6.1	3.18	0.95
Average values for the 3 models:			$^{calc,\,avg}\delta_{iso}$ 21.6 ppm			$^{calc,\,avg}\lvert C_Q\rvert$ 3.42 MHz			$^{calc,\,avg}\eta_Q$ 0.64

Structural analysis of Ca local environments in the a-CPP models

Table S4: Analysis of the average Ca…O bond distance, coordination number, and number of coordinated water ligands in 3 models of the amorphous $Ca_2P_2O_7.xH_2O$ phase (a-CPP, x ~ 4). Two different cut-off distances were chosen to describe the Ca coordination environment (2.7 and 3.0 Å).

	Model I					Model II					Model III				
	Coordination number		Average Ca…O distance		n H_2O	Coordination number		Average Ca…O distance		n H_2O	Coordination number		Average Ca…O distance		n H_2O
Cutoff	2.7 Å	3.0 Å	2.7 Å	3.0 Å	2.7 Å	2.7 Å	3.0 Å	2.7 Å	3.0 Å	2.7 Å	2.7 Å	3.0 Å	2.7 Å	3.0 Å	2.7 Å
Ca1	7	7	2.49	2.49	1	7	8	2.51	2.54	0	5	6	2.43	2.49	1
Ca2	6	6	2.35	2.35	3	6	6	2.40	2.40	2	5	5	2.29	2.29	2
Ca3	6	6	2.37	2.37	1	7	7	2.41	2.41	2	5	5	2.39	2.39	2
Ca4	6	6	2.40	2.40	2	5	6	2.36	2.43	1	5	6	2.37	2.45	2
Ca5	7	7	2.40	2.40	2	6	8	2.51	2.57	2	9	9	2.54	2.54	3
Ca6	6	6	2.43	2.43	3	6	6	2.37	2.37	4	7	7	2.45	2.45	4
Ca7	8	8	2.51	2.51	5	5	5	2.35	2.35	1	4	4	2.32	2.32	1
Ca8	7	7	2.46	2.46	4	6	7	2.36	2.42	4	6	8	2.43	2.56	2
Ca9	6	6	2.33	2.33	1	6	8	2.45	2.53	2	6	6	2.38	2.38	2
Ca10	6	6	2.45	2.45	2	6	7	2.41	2.49	2	6	6	2.41	2.41	3
Ca11	6	6	2.36	2.36	1	6	6	2.38	2.38	3	7	8	2.40	2.47	3
Ca12	6	6	2.36	2.36	0	5	5	2.37	2.37	0	6	7	2.43	2.48	1

Simulations using Czjzek (Gaussian Isotropic Model, GIM) and Gaussian isotropic chemical shift distributions.[19]

For both magnetic fields (20.0 and 35.2 T), the initial values of $C_Q(^{43}Ca)$, $\eta_Q(^{43}Ca)$ and $\delta_{iso}(^{43}Ca)$ were obtained by GIPAW calculations (12 Ca sites *per* AIMD model) (see Figure 3a/ in the main text). Following ref. 19, the GIM (Gaussian Isotropic Model) case of the Czjzek distribution was then used for each *individual* calcium site. GIM corresponds to a statistical distribution of charges around the observed nucleus. Such an assumption is *a priori* valid for ^{43}Ca. In Figure S4, various levels of Gaussian isotropic chemical shift distribution were added (from 0 ppm, *i.e.* GIM model, to 20 ppm).

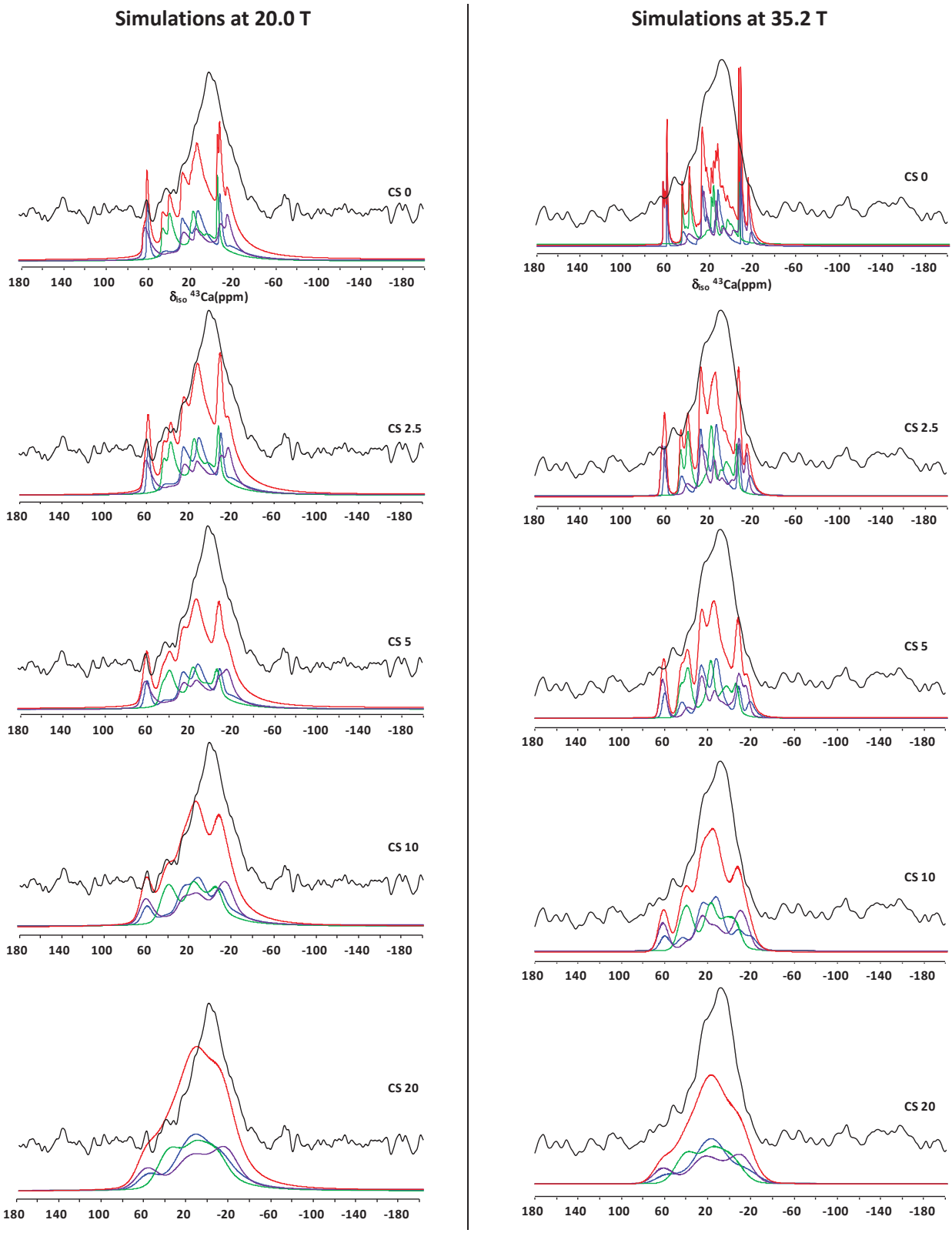

Figure S4. Czjzek and Gaussian isotropic chemical shift distributions for a-CPP at 20.0 and 35.2 T. CS: Gaussian isotropic chemical shift distribution in ppm. CS = 0 corresponds to the Czjzek model. CS = 10 (to 20 ppm) corresponds to a reasonable estimation.

References

[1] Gras, P.; Rey, C.; Marsan, O.; Sarda, S.; Combes, C. *Eur. J. Inorg. Chem.* **2013**, 5886.
[2] Colas, H.; Bonhomme-Coury, L.; Coelho Diogo, C.; Tielens, F.; Babonneau, F.; Gervais, C.; Bazin, D.; Laurencin, D.; Smith, M. E.; Hanna, J. V.; Daudon, M.; Bonhomme, C. *CrystEngComm,* **2013**, *15*, 8840.
[3] Gervais, C.; Laurencin, D.; Wong, A.; Pourpoint, F.; Labram, J.; Woodward, B.; Howes, A. P.; Pike, K. J.; Dupree, R.; Mauri, F.; Bonhomme, C.; Smith, M. E. *Chem. Phys. Lett*. **2008**, *464*, 42.
[4] Brinkmann, A.; Kentgens, A.P.M. *J. Phys. Chem. B* **2006**, 110, 16089.

[5] Gan, Z.; Kwak, H.-T. *J. Magn. Reson.* **2004**, *168*, 346.
[6] O'Dell, L. A. *Solid State NMR*, **2013**, *55-56*, 28.
[7] Gras, P.; Baker, A.; Combes, C.; Rey, C.; Sarda, S.; Wright, A. J.; Smith, M. E.; Hanna, J. V.; Gervais, C.; Laurencin, D.; Bonhomme, C. *Acta Biomater.* **2016**, *31*, 348.
[8] Tucker, M.G., Keen, D.A., Dove, M.T., Goodwin, A.L., Hui, Q, *J. Phys. Condens. Matter* **2007,** *19,* 335218
[9] Juhás, P.; Davis, T.; Farrow, C. L.; Billinge, S. J. L. *J. Appl. Cryst.* **2013**, *46*, 560.
[10] Farrow, C. L.; Juhas, P.; Liu, J. W.; Bryndin, D.; Boin, E. S.; Bloch, J.; Proffen, T.; Billinge, S. J. L. *J. Phys. Condens. Matter* **2007**, *19*, 335219
[11] T. Proffen, K. L. Page, S. E. McLain, B. Clausen, T. W. Darling, J. A. TenCate, S.-Y. Lee and E. Ustundag, *Zeitschrift für Krist. - Cryst. Mater.*, 2005, **220**, 1002–1008.
[12] Pickard, C. J.; Mauri, F. *Phys. Rev. B* **2001,** *63*, 245101.
[13] Giannozzi, P. B., S.; Bonini, Nicola; Calandra, M.; Car, R.; Cavazzoni, C.; Ceresoli, D.; Chiarotti, G. L.; Cococcioni, M.; Dabo, I.; Dal Corso, A.; Fabris, S.; Fratesi, G.; de Gironcoli, S.; Gebauer, R.; Gerstmann, U.; Gougoussis, C.; Kokalj, A.; Lazzeri, M.; Martin-Samos, L.; Marzari, N.; Mauri, F.; Mazzarello, R.; Paolini, S.; Pasquarello, A.; Paulatto, L.; Sbraccia, C. *J. Phys. Condens. Matter* **2009,** *21*, 395502-1-19.
[14] Troullier, N.; Martins, J. L. *Phys. Rev. B* **1991**, *43*, 1993.
[15] Kleinman, L.; Bylander, D. *Phys. Rev. Lett.* **1982**, *48*, 1425.
[16] Perdew, J. P.; Burke, K.; Ernzerhof, M. *Phys. Rev. Lett.* **1997**, *78*, 1396.
[17] Gervais C., Jones C., Bonhomme C., Laurencin D. *Acta Cryst.* **2017**, *C73*, 208.
[18] Pyykkö, P. *Mol. Phys.* **2008,** *106*, 1965.

[19] Neuville, D.R. ; Cormier L. ; Massiot D. *Geochim. Cosmochim. Acta* **2004**, 68, 5071.